ELSEVIER

Catalysis Today 54 (1999) 483–494

CATALYSIS TODAY

www.elsevier.com/locate/cattod

Reduction of NO_x over Fe/ZSM-5 catalysts: mechanistic causes of activity differences between alkanes

H.-Y. Chen, T. Voskoboinikov[1], W.M.H. Sachtler *

V.N. Ipatieff Laboratory, Center for Catalysis and Surface Science, Department of Chemistry, Northwestern University, Evanston, IL 60208, USA

Abstract

Fe/ZSM-5 catalysts prepared by sublimation of $FeCl_3$ onto H/ZSM-5 catalyze the selective reduction of NO_x by hydrocarbons to N_2. The order of the relative rates and N_2 yields obtained with different alkanes reveals a non-trivial chemistry. The maximum yield is lower for propane than for *n*-butane but about the same for *n*- and *iso*-butane. However, at temperatures below this maximum, the N_2 yield is higher for propane and *n*-butane than for *iso*-butane. Deposits are formed on the catalyst that contain N atoms in a low-oxidation state which are able to react with NO_2 to form N_2. TPO and FTIR results show that the amount and also the character of the deposits depend on the nature of alkanes. The change of the oxidation state of nitrogen from a high value in NO or NO_2 to a lower value in nitrile and amino groups of the deposit is rationalized by applying mechanistic concepts of organic chemistry, including the Beckmann rearrangement and fragmentation. FTIR spectra and the observed oxygen- and nitrogen-containing compounds by GC-MS are potential clues to the reaction mechanism.

Keywords: DeNO$_x$; SCR of NO$_x$; Fe/ZSM-5; Active catalyst deposits; Transformation of N^{4+} into N^{3-} adsorption complexes

1. Introduction

In a previous paper, we reported that the catalytic activity of Fe/ZSM-5 depends on the type of hydrocarbons used: methane is inactive, while propene is less active than propane or *iso*-butane [1]. The SCR mechanism over these catalysts was shown to include formation of a nitrogen containing deposit on the catalyst; its interaction with NO_2 ($NO + O_2$) yields N_2. Isotopic labeling showed that, in these N_2 molecules, one N atom comes from the deposit, the other from NO_2. A substantial fraction of the N_2 yield in the SCR of NO_x over Fe/ZSM-5 appears to be formed along this route. In the present paper, a more systematic study of the catalytic performance with different light alkanes will be reported and evidence of possible relevance for the formation of these deposits and their interaction with NO_2 will be presented.

2. Experimental

The Fe/ZSM-5 catalysts were prepared by our sublimation method; for the details of the preparation and characterization of the samples we refer to our earlier papers [2–4]. The parent ZSM-5 zeolite used in this work was obtained from UOP (lot # 13923, Si/Al = 14.2).

* Corresponding author. Tel.: +1-847-491-5263; fax: +1-847-467-1018
E-mail address: wmhs@nwu.edu (W.M.H. Sachtler)
[1] Present address: UOP Research Center, P.O. Box 5016, Des Plaines, IL 60017, USA.

0920-5861/99/$ – see front matter
PII: S0920-5861(99)00211-4

Catalytic tests were performed with 0.2 g Fe/ZSM-5 in powdered form in a micro-flow reactor at atmospheric pressure. The products were analyzed by on-line GC-TCD with Alltech 13X molecular sieve and Parapak Q columns. The feed gas containing 0.2% NO, 3% O_2 and the hydrocarbon adjusted to a flux of 0.8% carbon (0.27% C_3H_8, 0.2% *n*-C_4H_{10} or *i*-C_4H_{10}) with He as a diluent was passed through the catalyst bed with a total flow rate of 280 ml/min (GHSV = 42 000 h^{-1}). The temperature dependence of the catalytic performance was measured by raising the temperature stepwise from 200 to 500°C. Sampling was done 30 min after a preset temperature had been reached, the thus obtained activity may not represent a true steady state if catalyst performance changed with time. This time dependence was measured in separate runs at 300°C, in which case sampling was made every 5 min. After 3 h testing at a constant temperature, the catalyst was purged at 300°C for 30 min, and cooled to room temperature in flowing He (100 ml/min). The catalyst was subsequently subjected to temperature-programmed oxidation (TPO) in order to analyze any deposits that might have been formed on it during the 3-h run.

TPO was carried out with a 5% O_2/Ar flow of 60 ml/min and a temperature ramp rate of 8°C/min. After 500°C was reached, the temperature was held at this value for 30 min. The evolution of carbon dioxide ($M/e = 44$), water ($M/e = 18$) and nitrogen ($M/e = 28$) was monitored by mass spectrometry. The $M/e = 12$ and $M/e = 14$ signals, both indicate that CO formation during TPO runs is negligible. Therefore, to calculate the N_2 in the gas obtained by oxidizing the deposit, only the contribution of the $M/e = 28$ fragment from CO_2 was subtracted from the $M/e = 28$ signal [5].

Mass spectrometry, coupled to gas chromatography (GC-MS, Hewlett–Packard, G1800A, GCD system) was used to detect oxygen- and nitrogen-containing compounds. Products from the reaction at 200°C, the light-off temperature, were trapped in liquid N_2 for 30 min, separated on a 50-m PONA (cross-linked methyl silicone gum) capillary column with a temperature program from 35°C (5 min) to 150°C (15°C/min).

FTIR measurements were carried out on a Nicolet 60SX FTIR spectrometer equipped with a liquid N_2-cooled MCT detector. The Fe/ZSM-5 catalysts were pressed into self-supporting wafers of 8–10 mg/cm^2. The wafer was placed into a quartz cell sealed with NaCl windows, calcined in situ to 500°C, and then cooled to 200°C in flowing O_2/He (5%, 100 ml/min). In situ reaction measurements were carried out at 200°C under a flow of NO (0.5%), alkane (C_3H_8, *n*-C_4H_{10} or *i*-C_4N_{10}, 0.2%) , O_2 (3%) and He with a total flow rate of 100 ml/min. Spectra were recorded as a function of time upon exposing the calcined sample to the feed. Fifty scans were accumulated with a spectral resolution of 1 cm^{-1}. A reference spectrum of the calcined sample was subtracted from each spectrum.

3. Results

3.1. Catalytic activity and formation of by-products

Fig. 1 shows the temperature dependence of the N_2 yield using C_3H_8, *n*-C_4H_{10} and *i*-C_4H_{10} as reductants. The onset temperature of NO reduction is at ca. 200°C. The N_2 yield always increases initially with increasing temperature until it reaches a maximum, and is then followed by a decrease. The temperature at which the maximum N_2 yield is observed at the same carbon flux depends on the type of alkane used, it shifts upward in

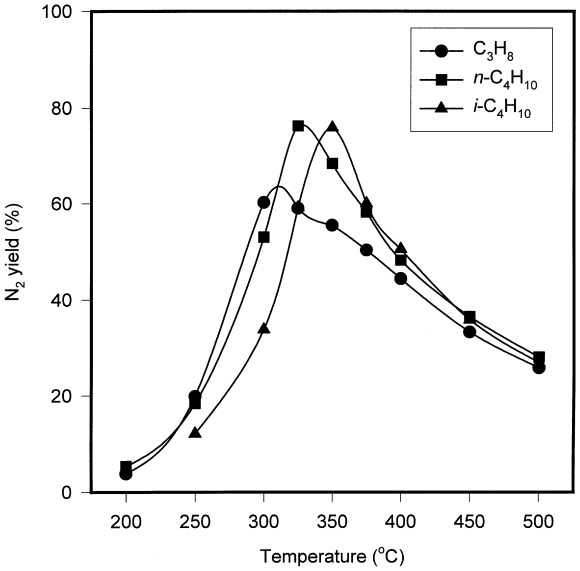

Fig. 1. N_2 yield as a function of temperature for different alkanes. Conditions: NO, 0.2%; O_2, 3%; C_3H_8, 0.27% (or *n*(*i*)-C_4H_{10}, 0.2%); GHSV 42 000 h^{-1}.

the order $C_3H_8 < n\text{-}C_4H_{10} < i\text{-}C_4H_{10}$. The maximum N_2 yield is about the same for $n\text{-}C_4H_{10}$ and $i\text{-}C_4H_{10}$, but it is lower for C_3H_8. This shows that propane is a less effective reductant for SCR of NO_x. Whereas in the descending branches above 375°C, the differences in N_2 yield are less obvious, the N_2 yield in the ascending branches is higher for C_3H_8 and $n\text{-}C_4H_{10}$ than for $i\text{-}C_4H_{10}$. This shows that H abstraction from the alkane is not necessarily a rate-limiting step. In addition to N_2, the effluent contains CO and CO_2, as reported previously [2]. Below 300°C, traces of N_2O were also detected; however, the concentration was too low for quantitative analysis by our on-line GC.

With C_3H_8, the N_2 yield does not change with time-on-stream in the whole temperature region. With $n\text{-}C_4H_{10}$ and $i\text{-}C_4H_{10}$, the same holds for the descending branch, but for the ascending branch, the N_2 yield is found to decrease with reaction time. Fig. 2 shows the N_2 yield at 300°C as a function of time-on-stream with $n\text{-}C_4H_{10}$ or $i\text{-}C_4H_{10}$ as the reductant. While the initial activity is roughly the same for both hydrocarbons, it clearly decreases more rapidly with $i\text{-}C_4H_{10}$. This deactivation is caused by the formation of an inactive deposit, as the color of the catalyst changes from yellow to gray. The presence of organic deposits

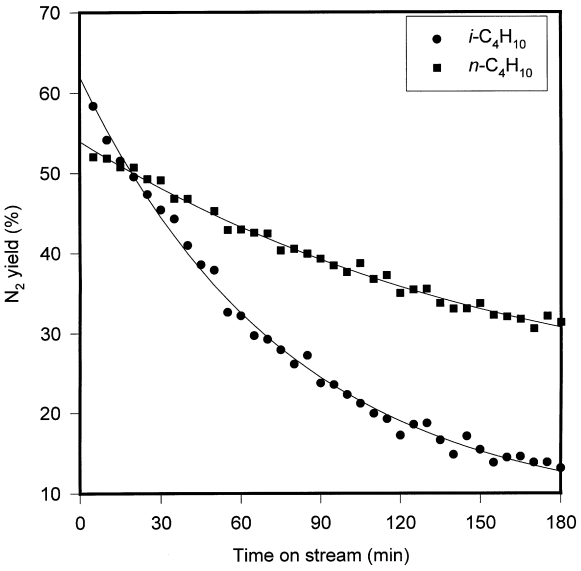

Fig. 2. N_2 yield as a function of time-on-stream for $n(i)$–C_4H_{10}. Conditions: NO, 0.2%; O_2, 3%; $n(i)$–C_4H_{10}, 0.2%; GHSV 42 000 h^{-1}, 300°C.

is confirmed by the TPO profiles of the catalysts after 3-h testing at 300°C, as shown in Fig. 3. With C_3H_8 as a reductant, there is virtually no CO_2 being detected during the TPO run (profile not shown). Evolution of CO_2 is observed with catalysts previously exposed to $n\text{-}C_4H_{10}$ or $i\text{-}C_4H_{10}$. Although the peak areas are rather similar, the shapes of the TPO profiles are different. For the deposit formed by using $n\text{-}C_4H_{10}$, one broad peak with a maximum temperature at 403°C was registered, but in the case of $i\text{-}C_4H_{10}$, an additional peak was recorded at lower temperatures ($T = 359$°C). This suggests that the nature of the deposits is different for $n\text{-}C_4H_{10}$ and $i\text{-}C_4H_{10}$. This conclusion is further supported by the differences between the H_2O and N_2 features in Fig. 3. From the peak areas, the relative amounts of deposit on the catalyst can be estimated: with $n\text{-}C_4H_{10}$, the ratio of CO_2/Fe is about 1.9, and the composition of the deposit corresponds to $CH_{0.75}N_{0.14}O_x$; with $i\text{-}C_4H_{10}$, the CO_2/Fe ratio is about 2.0, and the composition formula is $CH_{1.04}N_{0.22}O_x$. (In these calculations, the first H_2O peak which is due to desorption from the zeolite has been disregarded.) Clearly, the deposit formed with $n\text{-}C_4H_{10}$ is 'harder' and contains less nitrogen than the deposit formed with $i\text{-}C_4H_{10}$.

In order to get some clues for the chemistry converting alkanes with NO_2 into a deposit containing N atoms in low electrochemical valence, we have tried to identify potential reaction intermediates. For this purpose, catalytic tests were carried out with dry feeds of different alkanes at 200°C; the effluent gas was trapped in liquid N_2, subsequently heated to RT and analyzed by GC-MS. Fig. 4 shows the GC-MS analysis results. The first peak contains mainly O_2, N_2, CO, CO_2, NO and N_2O. These gases cannot be well separated by the column. Also, the retention times for C_3H_8, H_2O and formaldehyde(CH_2O) are very similar, so that their peaks overlap; the combined peak will be labeled 'C_3H_8'. In a separate experiment, we condensed the effluent at 0°C and analyzed the liquid condensate by GC-MS. Formaldehyde and acetic acid were identified as oxygenated products for all three alkanes.

In the condensate trapped at liquid N_2, acetone was found with $i\text{-}C_4H_{10}$, but not with C_3H_8 or $n\text{-}C_4H_{10}$. With C_3H_8 (Fig. 4(A)) hydrogen cyanide (HCN) and ethane dinitrile (NCCN) were found as major nitrogen-containing products. Hydrogen chloride

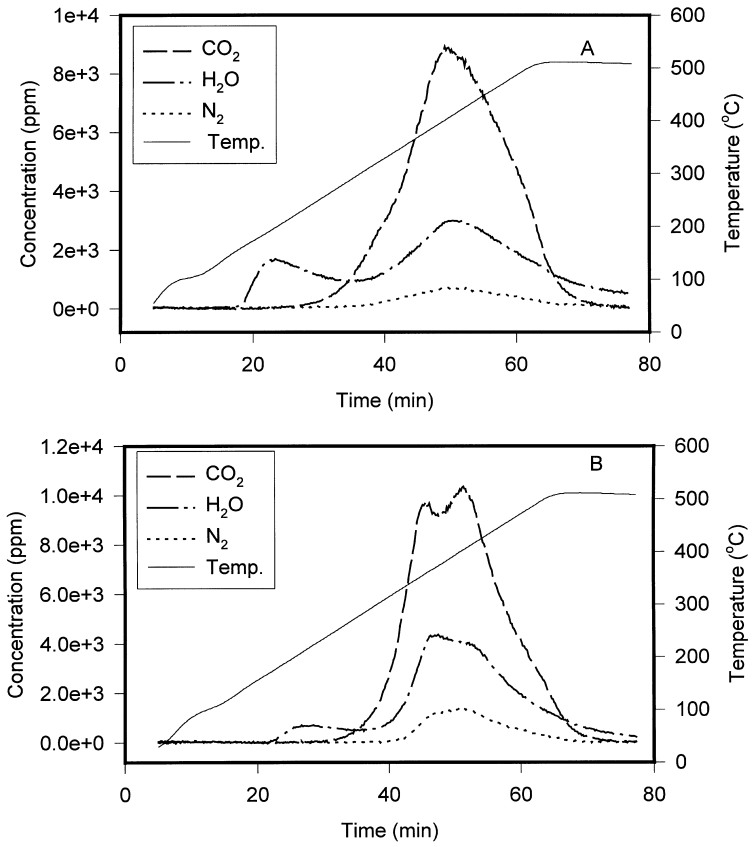

Fig. 3. TPO of Fe/ZSM-5 sample after catalytic activity test at 300°C for 3 h with (A) n-C_4H_{10}, and (B) i-C_4H_{10} as a reductant.

(HCl) and cyan chloride (ClCN) were also detected. The chlorine is presumably a remnant from the catalyst preparation with $FeCl_3$.

Remarkable differences were found for n-C_4H_{10} (Fig. 4(B)) and i-C_4H_{10} (Fig. 4(C)). With n-C_4H_{10}, acetonitrile and acrylonitrile were detected in addition to HCN and NCCN. With i-C_4H_{10}, a rather significant peak of methacrylonitrile was observed that was absent with the other two alkanes. In addition, acetonitrile and HCN were detected, but virtually no NCCN was found. Traces of other hydrocarbons (C_3H_8, n-C_4H_{10} or i-C_4H_{10}) were detected when n-C_4H_{10} or i-C_4H_{10} was used; these are not reaction products but impurities in the feed gas.

3.2. FTIR

In situ FTIR was used to identify IR-active groups that are deposited on the catalyst surface during the SCR reaction. Spectra were registered at 200°C as a function of time upon exposing the catalyst to a feed of 0.5% NO + 0.2% C_xH_y + 3% O_2. After 30 min, the hydrocarbon in this mixture was replaced by an equal amount of helium.

3.2.1. C_3H_8+NO+O_2

As shown in Fig. 5, a negative band appeared at 3666 cm^{-1} when the catalyst was exposed to the feed, suggesting that OH groups disappeared. Its wave number is between those typical for Si-OH groups (3710 cm^{-1}) and Brønsted acid sites (3605 cm^{-1}). A band at 3690 cm^{-1} was observed by Zecchina et al. [6] over an MFI-type ferrisilicalite, it was assigned to OH groups present in small clusters of extraframework iron species. We, therefore, assume that the 3666 cm^{-1} band can be assigned to OH groups attached to iron ions, such as $[HO\text{-}Fe\text{-}O\text{-}Fe\text{-}OH]^{2+}$ that we proposed previously [2–4]. Adsorption of

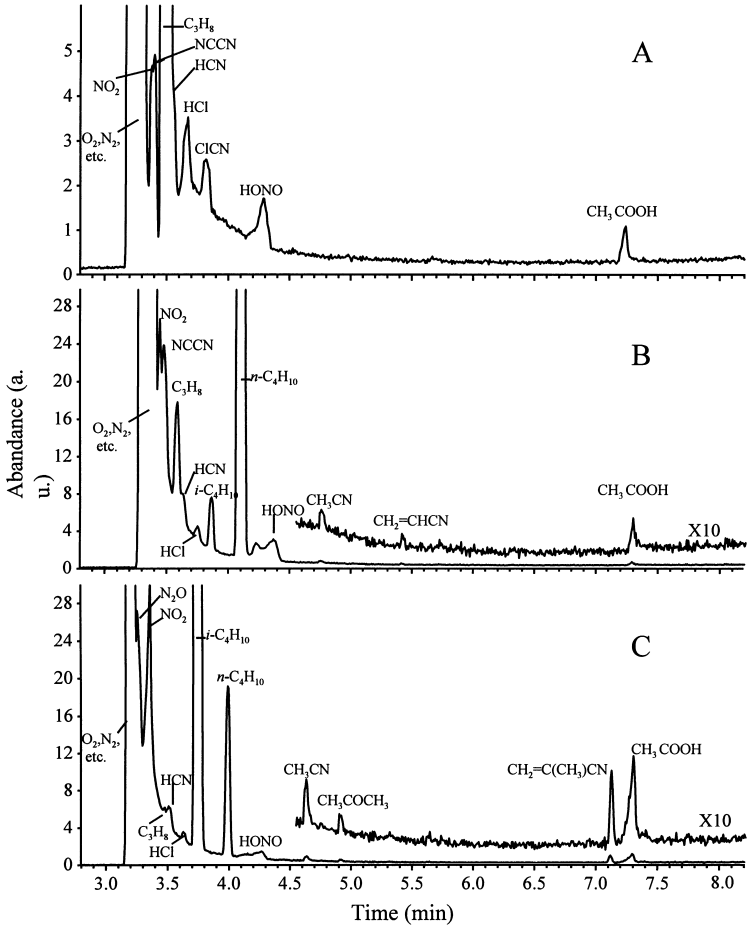

Fig. 4. GC-MS chromatogram of products in the SCR of NO with: (A) C_3H_8; (B) n-C_4H_{10}; (C) i–C_4H_{10} as a reductant.

mononitrosyl (1878 cm^{-1}[1]) and nitro/nitrate (1625, 1570 cm^{-1} [1]) groups on the iron sites will perturb this OH group, so that a negative band will result at this wave number. In addition, several weak bands were observed. Bands in the region 3000–2800 cm^{-1} are due to the C–H stretching vibrations of adsorbed C_3H_8 [7]. A band at 2131 cm^{-1} has recently been assigned to NO^+ ions occupying Brønsted acid sites in the zeolite [8]. A weak band at 2255 cm^{-1} became obvious after 30 min. It could be assigned to a cyanide group at an iron site or to an organic nitrile group. A shoulder at 1543 cm^{-1} appeared at 2 min, which was, however, masked after 10 min. This band could be attributed to the NO_2 asymmetric stretching vibration in $(CH_3)_2CHNO_2$ [9]. The corresponding symmetric stretching vibration of the $–NO_2$ group was observed at 1379 cm^{-1}. The latter band overlapped with a band at 1357 cm^{-1}, which might be attributed to a carbonate [1]. In the double bond (C=O, C=N, N=O, etc.) region, a weak, broad band at 1678 cm^{-1} was evident; it became less obvious after C_3H_8 was eliminated. A band at 1435 cm^{-1} grew with time; it did not decline when C_3H_8 was eliminated. This band can be attributed to a carbonate group [1].

Fig. 5 shows that, with C_3H_8 as a reductant, the catalyst surface is rather ‘clean’; nearly no carbonaceous deposit was formed under reaction conditions, which is in agreement with the TPO result. This is also consistent with the catalytic-activity result obtained in the micro-flow reactor, i.e. no decline of the N_2 yield was observed with time-on-stream.

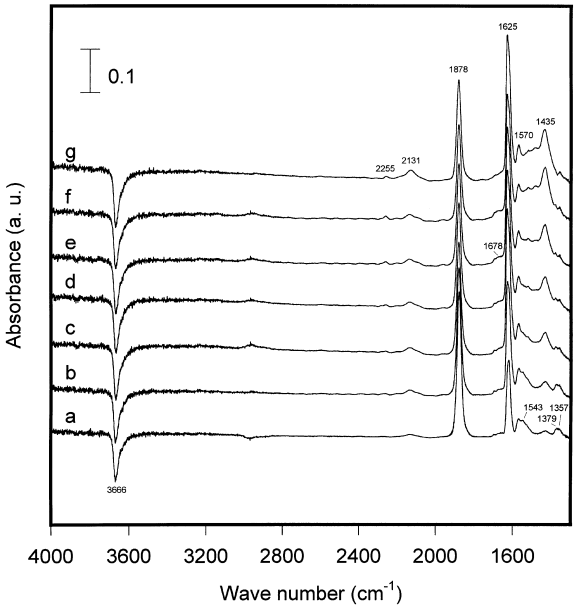

Fig. 5. FTIR spectra taken at 200°C upon exposing Fe/ZSM-5 sample to a flow of NO 0.5% + O_2 3% + C_3H_8 0.2% + He for 2 (a); 5 (b); 10 (c); 15 (d); 20 (e); and 30 min (f); following (f), C_3H_8 was replaced by He for 30 min (g).

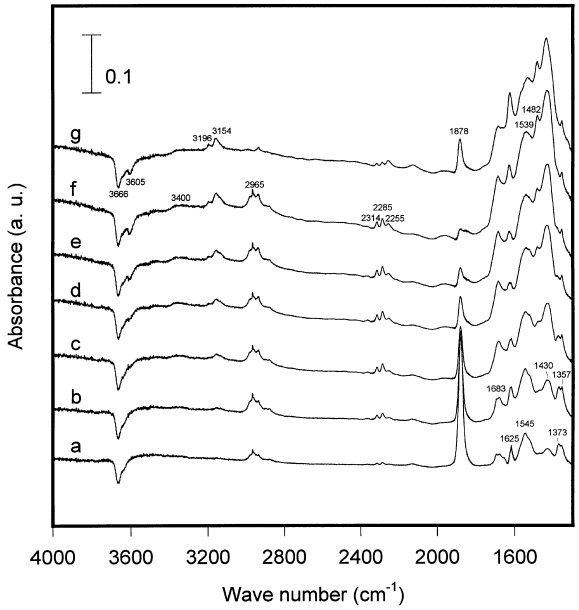

Fig. 6. FTIR spectra taken at 200°C upon exposing Fe/ZSM-5 sample to a flow of NO 0.5% + O_2 3% + n-C_4H_{10} 0.2% + He for 2 (a); 5 (b); 10 (c); 15 (d); 20 (e); and 30 min (f); following (f), n-C_4H_{10} was replaced by He for 30 min (g).

3.2.2. n-C_4H_{10} + NO + O_2

Fig. 6 shows that after 2 min (spectrum *a*), an intensive band appeared due to a mononitrosyl group (1878 cm^{-1}). Simultaneously, a negative band emerges at 3666 cm^{-1}, similar to the case with C_3H_8. However, the intensity of the band at 1625 cm^{-1} is much lower than in spectrum *a* in Fig. 5, indicating a higher reactivity of n-C_4H_{10} toward the nitro/nitrate group. This reaction might result in the formation of nitro-butane, to which the bands at 1545 cm^{-1} ($\gamma_{N=O}$ asym.) and 1373 cm^{-1} ($\gamma_{N=O}$ sym.) are ascribed. At the same time, butane nitrite might be formed; the N=O stretching vibration of organic nitrites has been reported in the 1610–1685 cm^{-1} region [9]. The band at 1683 cm^{-1} in Fig. 6 may contain a contribution from butane nitrite. Of course, other double bonds, such as C=N and C=O may also contribute. The band intensity of the mononitrosyl decreased quickly with exposure time, meanwhile, intensive bands in the 1300–1800 cm^{-1} region grew very quickly, and a broad band centering at 3154 cm^{-1} with a shoulder at 3196 cm^{-1} emerged. The totality of these bands indicates formation of a carbonaceous deposit on the catalyst. The broad band at 3154 cm^{-1} could be assigned to a C–H stretching vibration from unsaturated groups [10]. The shoulder at 3196 cm^{-1} might be due to an N–H stretching vibration (see below). The broad bands in the 1300–1800 cm^{-1} region show a few maxima for which unambiguous assignment is difficult. Here, we tentatively assign the band at 1683 cm^{-1} to the stretching vibration of a double band, such as N=O, C=O and C=N. The band at 1625 cm^{-1} is most probably due to nitro groups on iron [1]. The band at 1539 cm^{-1} is likely due to a C=C stretching vibration, while the band at 1482 cm^{-1} could be attributed to C–H deformation of the deposit [11]. The bands at 1430 cm^{-1} and 1357 cm^{-1} might be due to carbonate. Interestingly, simultaneously with the formation of the carbonaceous deposits, a negative band appeared at 3605 cm^{-1}, suggesting that Brønsted acid sites (as discussed previously [2], ∼20% Brønsted acid sites were regenerated after hydrolysis) were consumed. This interaction, probably a protonation of unsaturated hydrocarbons, led to the appearance of a very broad band centering at 3400 cm^{-1}. The deposit blocks the sites onto which NO is adsorbed as is evidenced by the intensity decrease of the bands due to mononitrosyl groups. However, this site-blocking effect remains

incomplete, the intensity of the band at 1878 cm^{-1}, and also of the band at 1625 cm^{-1} (nitro group), does not reduce to zero even after 30 min. These intensities increased again when *n*-C_4H_{10} was eliminated from the feed, so that the organic deposit was oxidized. In the triple band region 2100–2300 cm^{-1}, a doublet at 2314 cm^{-1} and 2285 cm^{-1} emerged when the catalyst was exposed to the feed. Its intensity increased with time, meanwhile, another band at 2255 cm^{-1} emerged. When *n*-C_4H_{10} was removed from the feed, the intensity of the doublet decreased, but almost no change was observed for the band at 2255 cm^{-1}. Based on the spectra of adsorbed model compounds (see below), the doublet at 2314 cm^{-1} and 2283 cm^{-1} can be assigned to the CN stretching vibration of an adsorbed saturated aliphatic nitrile, the band at 2255 cm^{-1} being assigned to the CN stretching vibration of a conjugated nitrile.

3.2.3. *i*-C_4H_{10}+*NO*+O_2

As with C_3H_8 or *n*-C_4H_{10}, a mononitrosyl group (1878 cm^{-1}) was observed at 2 min, together with a negative band at 3666 cm^{-1} (Fig. 7(a)), but the band at 1625 cm^{-1} that was assigned to a nitro group on iron was hardly visible, suggesting an even higher reactivity of *i*-C_4H_{10} toward the nitro/nitrate groups. In the same spectrum, bands at 1542 cm^{-1} and 1380 cm^{-1} which might be caused by $(CH_3)_3C–NO_2$ were visible. The band at 1542 cm^{-1} could also be assigned to the N=O stretching mode from $(CH_3)_3C–NO$ [9]. In the double-bond region, a band at 1680 cm^{-1} appeared which may contain a contribution from $(CH_3)_3C–ONO$. It is reasonable to assume that $(CH_3)_3–NO_2$, $(CH_3)_3C–NO$ and $(CH_3)_3C–ONO$ could be initial products of the reaction of *i*-C_4H_{10} with the adsorbed NO_y complexes. After a longer exposure time, the intensity of the mononitrosyl group decreased dramatically and vanished after 15 min. Intensive bands in the 1300–1800 cm^{-1} region, together with a broad band centering at 3145 cm^{-1}, grew quickly. Simultaneously, a negative band at 3605 cm^{-1} and a very broad band centering at 3400 cm^{-1} appeared. These results suggest that the deposit formed with *i*-C_4H_{10} interacted vigorously with Brønsted acid sites. It eventually blocked the iron sites completely, so that no more mononitrosyl and nitro/nitrate groups were detectable after 15 min. This site blocking was so strong — or in other words, the deposit was so inactive — that these bands did not re-appear upon interrupting the *i*-C_4H_{10} flow for 30 min. As in the case of *n*-C_4H_{10}, a few maxima (1680, 1564, 1481, 1440, 1356 cm^{-1}) could be distinguished, but they were not at exactly the same position. The intensity of the band at 1680 cm^{-1} was higher than in the case of *n*-C_4H_{10}. The band at 1564 cm^{-1} appeared at higher frequency than the corresponding band for *n*-C_4H_{10} (1539 cm^{-1}). Both maxima at 1680 cm^{-1} and 1564 cm^{-1} decline when *i*-C_4H_{10} was omitted from the gas flow.

In the triple-bond region, a band at 2255 cm^{-1}, which could be assigned to a conjugated nitrile (see below), appeared immediately upon exposing the catalyst to the feed. Its intensity increased quickly and reached its maximum after 15 min. Meanwhile, a shoulder at 2238 cm^{-1} emerged, which could be assigned to the C≡N vibration in a polymer (see below). Upon further increasing the exposure time, the intensity of the band at 2255 cm^{-1} decreased while the band at 2238 cm^{-1} became predominant.

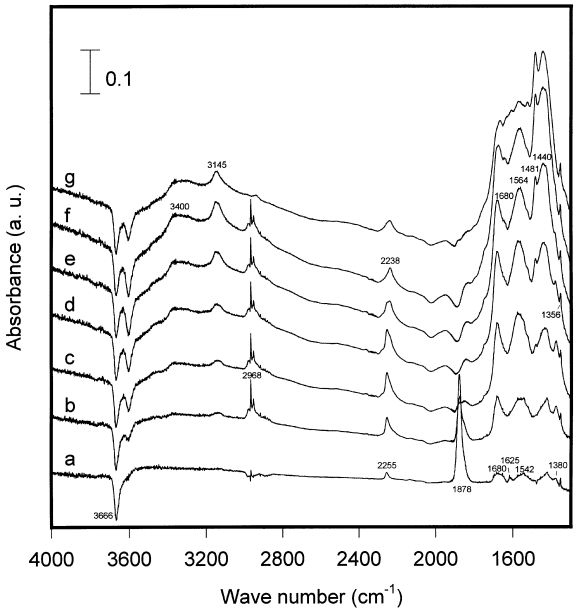

Fig. 7. FTIR spectra taken at 200°C upon exposing Fe/ZSM-5 sample to a flow of NO 0.5% + O_2 3% + *i*-C_4H_{10} 0.2% + He for 2 (a); 5 (b); 10 (c); 15 (d); 20 (e); and 30 min (f); following (f), *i*-C_4H_{10} was replaced by He for 30 min (g).

3.2.4. Spectra of adsorbed model compounds

IR bands in the triple bond region 2100–2300 cm^{-1} have been observed by numerous researchers [12–23]. However, the assignment of these bands is controversial. To make an unambiguous assignment, we recorded in Fig. 8 the IR spectra of some adsorbed model compounds.

Fig. 8(a–c) are the spectra for acetonitrile as an adsorbate. At room temperature, a doublet appeared at 2316 and 2289 cm^{-1} (spectrum *a*). This complex is rather stable. Upon heating to 200°C under He flow, the doublet remained intact with only a slight shift to 2314 cm^{-1} and 2285 cm^{-1}, respectively, and a small change of the relative intensities (spectrum *b*). An oxidizing atmosphere did not change the spectrum at 200°C (spectrum *c*). Interestingly, the band position and the relative intensity of the doublet are exactly the same as those in Fig. 6. Therefore, we assign the bands to the CN stretching vibration in acetonitrile, or more generally to saturated aliphatic nitriles. Fig. 8(d) is the spectrum of adsorbed methacrylonitrile, a single band was observed at 2255 cm^{-1}. Thus, we assign the band at 2255 cm^{-1} in Figs. 6 and 7 to the CN stretching vibration of a conjugated nitrile, such as acrylonitrile, or methacrylonitrile. Fig. 8(e–g) are the spectra using ethyl isocyanate (C_2H_5NCO) as an adsorbate. Three bands at 2377 cm^{-1}, 2329 cm^{-1} and 2232 cm^{-1} were observed at room temperature. This compound is not stable on the catalyst. Upon heating to 200°C in a He flow the bands at 2329 cm^{-1} disappeared, and the intensity of the bands at 2377 and 2332 cm^{-1} decreased, while two new bands at 2273 cm^{-1} and 2211 cm^{-1} developed. Under flowing O_2, the bands at 2377 cm^{-1} and 2232 cm^{-1} disappeared. However, none of the above bands was observed in the spectra shown in Figs. 5–7. So, it seems that, with light alkanes as reductants and under our reaction conditions, isocyanates are not present at the surface of Fe/ZSM-5.

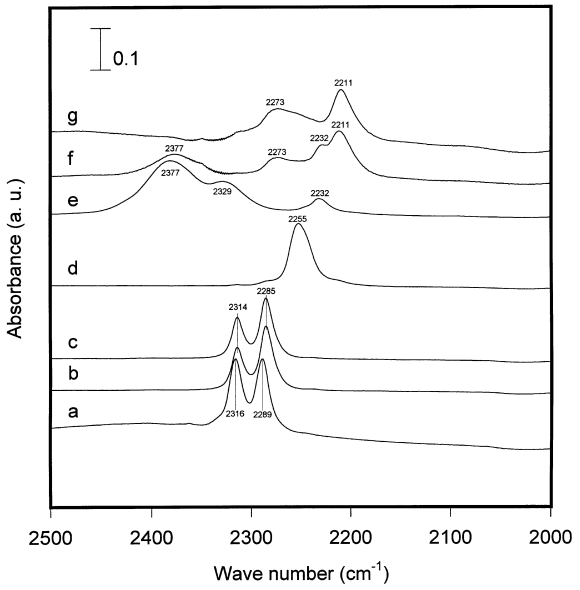

Fig. 8. FTIR spectra of adsorbed CH_3CN at room temperature (a), at 200°C in flowing He (b), and at 200°C in flowing O_2 (c); of adsorbed CH_2=C(CH_3)–CN at 200°C in flowing O_2 (d); and of adsorbed C_2H_5NCO at RT (e), at 200°C in flowing He (f), and at 200°C in flowing O_2 (g).

4. Discussion

The catalytic performance and the FTIR spectra consistently show that the reaction path of SCR of NO_x over Fe/ZSM-5 depends on the type of alkane used. Obvious differences exist between C_3H_8, *n*-C_4H_{10} and *i*-C_4H_{10}. This illustrates the role of organic chemistry in the SCR reaction. In this chapter we shall, therefore, compare the putative intermediates of hypothetical reactions at the catalyst surface with the observed IR bands and the TPO results.

In previous papers [1,24], we have shown that the first step for SCR of NO_x over Cu/ZSM-5, Co/ZSM-5 and Fe/ZSM-5 is the formation of adsorbed NO_y complexes. Such groups interact with hydrocarbons possibly via a free-radical mechanism. The *a* spectra in Figs. 5–7 indicate that the rate of this interaction between the nitro/nitrate group and the hydrocarbon increases in the following order: *i*-C_4H_{10} > *n*-C_4H_{10} > C_3H_8. This is consistent with the well-known chemistry: formation of a tertiary carbon radical is easier than that of a secondary one, and *n*-C_4H_{10} has two secondary carbon positions, while C_3H_8 has only one.

It is reasonable to assume that these hydrocarbon radicals react further with NO_x or the adsorbed NO_y complexes to form organic nitrite, nitroso or nitro compounds. Such compounds have been proposed to be intermediates for the SCR of NO_x with hydrocarbons by a number of researchers. However, only a few addressed how these compounds could further react with

other reactants forming N_2 [16–18,24–31]. As the following chemistry strongly depends on the nature of the hydrocarbons, we will discuss it separately for the three alkanes studied here.

4.1. $C_3H_8+NO+O_2$

The combination of a secondary propyl radical with NO_2 will likely result in the formation of 2-nitropropane. The IR spectra of aliphatic nitro compounds show the asymmetric and the symmetric vibrations of the nitro group in the spectral regions 1500–1600 and 1300–1390 cm^{-1} [9]. IR bands at 1545 and 1387 cm^{-1} in Fig. 5 confirm that an organic nitro compound was formed on the catalyst. Since α-H is present, it will take part in a tautomeric equilibrium with its aci-nitro form [32]:

$$(CH_3)_2CH\text{-}N^{\oplus}(=O)(O^{-}) \rightleftharpoons (CH_3)_2C{=}N^{\oplus}(OH)(O^{-}) \quad (1)$$

Hydrolysis of aci-nitropropane, also called the *Nef reaction*, will produce N_2O and a carbonyl compound:

$$(CH_3)_2C{=}N^{\oplus}(OH)(O^{-}) \rightarrow (CH_3)_2C{=}O + NOH \quad (2)$$

$$2NOH \rightarrow N_2O + H_2O \quad (3)$$

Over Fe/ZSM-5, this nitro compound is likely to dissociate into 2-nitrosopropane and oxygen, with the latter bonded to iron. 2-Nitrosopropane, which can also be formed by the combination of *sec*-propyl radical with NO, is known to spontaneously isomerize to its oxime:

$$(CH_3)_2C{=}HNO \rightarrow (CH_3)_2C{=}N\text{–}OH \quad (4)$$

The chemistry of this oxime on Cu/ZSM-5 was studied in detail by Beutel et al. [25]. Acetone oxime gives an IR band at 1661 cm^{-1}, attributed to the C=N stretching vibration [33]. In Fig. 5, a weak band at about 1678 cm^{-1} was found, which may contain a contribution from this oxime.

Hydrolysis of the oxime is known to give hydroxylamine:

$$(CH_3)_2C{=}N\text{–}OH + H_2O \rightarrow (CH_3)_2C{=}O + H_2N\text{–}OH \quad (5)$$

Hydroxylamine is a well-known reductant, it could react with NO_x forming N_2.

Another possibility is the Beckmann rearrangement of the oxime to N-methyl acetamide:

$$(CH_3)_2C{=}N\text{–}OH \rightarrow CH_3C(O)\text{–}N\text{–}CH_3 \quad (6)$$

which hydrolyzes to methylamine and acetic acid:

$$CH_3C(O)\text{–}NH\text{–}CH_3 + H_2O \rightarrow CH_3NH_2 + CH_3COOH \quad (7)$$

The amine will readily react with NO_2 leading to N_2 via a diazo compound.

On the other hand, *N*-methyl acetamide could also react with HONO:

$$CH_3C(O)\text{–}NH\text{–}CH_3 + HONO \rightarrow CH_3C(O)\text{–}N(NO)\text{–}CH_3 + H_2O \quad (8)$$

$$CH_3\text{-}C(=O)\text{-}N(\text{-}CH_3)(\text{-}N{=}O) \rightarrow CH_3\text{-}C(=O)\text{-}O\text{-}N{=}N\text{-}CH_3 \rightarrow CH_2{=}\overset{\oplus}{N}{=}\overset{\ominus}{N} + CH_3COOH \quad (9)$$

Decomposition of this diazo compound will form N_2.

For the Beckmann rearrangement, the formation of ions, their migration and recombination must occur simultaneously. However, steric limitations in the ZSM-5 zeolite structure may inhibit this reaction. Some of the ions may react with other nearby active agents, such as O_2, or NO_x. In that case, fragmentations could occur such as:

$$(CH_3)_2C{=}N\text{–}OH + \tfrac{1}{2}O_2 \rightarrow CH_3\text{–}CN + CH_2O + H_2O \quad (10)$$

Acetonitrile could react further with NO_y or NO_x leading to the formation of HCN and/or NCCN.

4.2. $n\text{-}C_4H_{10}+NO+O_2$

When n-C_4H_{10} is used instead of C_3H_8, a similar chemistry can be assumed. However, additional effects should also be considered due to the longer carbon chain. Decomposition of 2-nitrobutane is possible, since an adjacent secondary carbon is

available:

$$CH_3–CH_2–CH(NO_2)–CH_3 \rightarrow CH_3–CH{=}CH–CH_3 + HONO \quad (11)$$

Also for the fragmentation of 2-butanone oxime there exist two possibilities:

$$CH_3CH_2C(CH_3){=}N–OH \rightarrow CH_2{=}CH_2 + CH_3CN + H_2O \quad (12)$$

$$CH_3CH_2C(CH_3){=}N–OH + \tfrac{1}{2}O_2 \rightarrow CH_3CH_2CN + CH_2O + H_2O \quad (13)$$

Reactions (11) and (12), both lead to the formation of olefins. It is well known that these strongly interact with the Brønsted acid sites and easily form oligomers on the catalyst.

Propionitrile could react further with NO_y or NO_x, one possibility being the abstraction of hydrogen leading to the formation of acrylonitrile. Since acrylonitrile has a conjugated structure, it is more stable than a saturated nitrile. Nitrile groups are strongly adsorbed by Lewis acid sites, thus blocking the Fe sites of Fe/ZSM-5. (Co-)polymerization of adsorbed nitriles and olefins will result in the formation of deposits on the catalyst.

4.3. *i*-C_4H_{10}+*NO*+O_2

With *i*-C_4H_{10}, a free radical will easily be formed and it will react with NO_x forming tertiary nitro and/or nitroso compounds. The subsequent reactions will, however, be different from that of 2-nitro-butane, because there is no α-H available. A possible reaction that may occur with 2-methyl-2-nitropropane is the decomposition:

$$(CH_3)_3C–NO_2 \rightarrow (CH_3)_2C{=}CH_2 + HONO \quad (14)$$

by which an olefin is formed.

On the other hand, the nitro group could be considered as an active group to activate the primary carbon, so that it may react further with HONO:

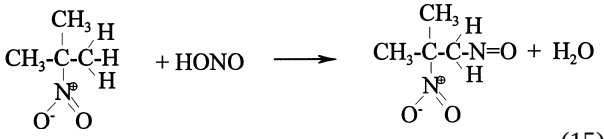

(15)

Once a nitroso group is attached to the terminal carbon atom, further reactions will be similar to those discussed above, leading to N_2 formation.

Another possible product that could be formed from the same compounds is methacrylonitrile:

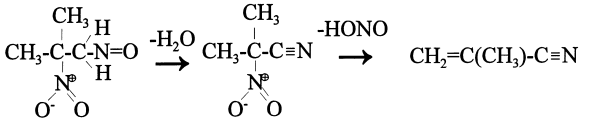

(16)

This reaction path seems to be supported by the present FTIR spectra (Fig. 7) which show a band at 2255 cm^{-1} assigned to a conjugated nitrile. This band appeared immediately when the catalyst was exposed to the feed, its intensity increased rapidly.

Methacrylonitrile is known for its strong propensity to polymerize. This is the most likely cause for the observed decline in intensity of the band attributed to conjugated nitriles after 15 min. At the same time, a band appears at 2238 cm^{-1}, which could be assigned to the CN vibration in a polymer. This polymer will eventually block the iron sites, which will lead to suppression of the oxidation of NO to NO_2 that is catalyzed by iron. Indeed, fast deactivation was observed in this reaction system as shown in Fig. 2.

Of course, the chemistry discussed above is oversimplified. Much more complicated reaction pathways may occur under reaction conditions. However, the crucial point is that a compound, such as NO or NO_2, with a high formal oxidation state of the N atom, is rearranged to a state in which the N atom has a lower level of oxidation so that it can form a new N/N bond with another NO_2. The examples shown above illustrate that this necessary change in formal oxidation state of the N atom can be achieved by oxidizing an adjacent methylene or methine group.

With the above-mentioned chemistry in mind, the effect of different alkanes on the catalytic activity over Fe/ZSM-5 for the SCR of NO_x can be rationalized as follows:

When C_3H_8 is used as a reductant, the rate-limiting step seems to be the activation of the hydrocarbon, i.e. C_3H_8 reacts with the NO_y groups forming a *sec*-propyl radical. Once it is formed, this radical will combine with NO_x forming 2-nitroso/nitro-propane. Since an α-H atom is present in the latter compound, it can easily un-

dergo isomerization and hydrolysis as discussed above. Thus, the impinging nitrogen atom ex $NO_x$is reduced to a low-oxidation state. As subsequent reduction with NO_2 leads to the release of N_2 [1], no N-containing deposit will be built up on the catalyst surface. Also, olefin formation from C_3H_8 would be unlikely. This leaves the catalyst surface rather 'clean', no coke will be formed on the catalyst under reaction conditions. This conclusion is supported by the present data on catalyst activity, as well as the TPO and FTIR results.

When *n*-C_4H_{10} is used as a reductant, reaction with the NO_y complexes will be faster than with C_3H_8, since two secondary carbon atoms are available in *n*-C_4H_{10}. Again, α-H atoms are available in the obtained 2-nitroso/nitro-butane, so basically the same chemistry can be applied and an active N-containing compound can be easily formed. However, a fast reaction between *n*-C_4H_{10} and NO_y complexes will deplete the latter groups which are also needed for the N_2 formation step [1]. Therefore, N-containing compounds will accumulate on the catalyst. This is confirmed by the spectra in Fig. 6. Also, owing to the longer carbon chain in *n*-C_4H_{10}, olefins can be formed as shown above. They will be strongly adsorbed on the Brønsted acid sites and form coke. They might also co-polymerize with the N-containing compounds forming catalyst deposits which will block the active sites. As a result, the catalyst activity with *n*-C_4H_{10} decreases with time on stream at lower temperatures, i.e. in the ascending branch of the activity test curve where the hydrocarbon conversion is lower than 100% (see Figs. 1 and 2).

When *i*-C_4H_{10} is used as a reductant, the presence of the tertiary carbon atom thoroughly increases the reactivity of the molecule with the NO_y groups. Unlike the case of C_3H_8 or *n*-C_4H_{10}, no α-H is present in the resulting nitroso/nitro compound; as a consequence, subsequent valence lowering steps become difficult. The intermediates will, therefore, accumulate on the catalyst. Under actual reaction conditions, they will decomposed or react with other compounds. Unsaturated organic nitriles, such as methacrylonitrile, are suggested by the GC-MS results in Fig. 3(B) and also the FTIR spectra in Fig. 7. Methacrylonitrile readily polymerizes and a deposit will be quickly formed which blocks the iron sites. As a result, the reduction rate decreases very rapidly with *i*-C_4H_{10} at temperatures in the ascending branch, where surface cleaning by deposit combustion is incomplete (Figs. 1 and 2). Since the deposit is mainly formed by a polymerization process, it contains more nitrogen and hydrogen atoms per C atom, but it is less reactive than the deposit from *n*-C_4H_{10}.

As the reaction steps in which the valence of the N atom is lowered require participation of an adjacent methylene or methine group, some of the partially oxidized hydrocarbon fragments will not be active reductants. This could explain why the maximum yield is lower for C_3H_8, but about the same for *n*-C_4H_{10} and *i*-C_4H_{10}, when the same carbon flux is fed.

5. Conclusion

Over Fe/ZSM-5 catalysts prepared by subliming $FeCl_3$ onto H/ZSM-5, the maximum N_2 yield in the SCR of NO_x at constant carbon flux is lower for C_3H_8 than *n*-C_4H_{10}, but about the same for *n*-C_4H_{10} and *i*-C_4H_{10}. However, at temperatures below this maximum, the N_2 yield is higher for C_3H_8 and *n*-C_4H_{10} than for *i*-C_4H_{10}. Formation of a deposit at low temperature was observed with *n*-C_4H_{10} and *i*-C_4H_{10}, but not with C_3H_8. TPO and FTIR results show that different deposits are formed with either alkane. Potential reaction paths for the SCR of NO_x have been proposed; a crucial point is that compounds with N atoms in a high oxidation state are converted to compounds with N atoms in a lower oxidation state. This conversion is basically achieved by oxidation of an adjacent methylene or methine group. As shown elsewhere [1,25], by means of labeled compounds, N–N bonds are formed by reaction of NO_2 with a surface compound containing an N atom in a low valence state, for instance an amine or amide. This appears to be the major route for the formation of N_2.

Acknowledgements

Financial support from the Director of the Chemistry Division, Basic Energy Sciences, U.S. Department of Energy, Grant DE-FGO2-87ER13654, is gratefully acknowledged.

References

[1] H.-Y. Chen, T. Voskoboinikov, W.M.H. Sachtler, J. Catal. 180 (1998) 171.
[2] H.-Y. Chen, W.M.H. Sachtler, Catal. Today 42 (1998) 73.
[3] H.-Y. Chen, W.M.H. Sachtler, Catal. Lett. 50 (1998) 125.
[4] T. Voskoboinikov, H.-Y. Chen, W.M.H. Sachtler, Appl. Catal. B 19 (1998) 279.
[5] A. Corna, R. Massot (Eds.), Compilation of Mass Spectroscopy Data, Heyden, London, 1966.
[6] A. Zecchina, F. Geobaldo, C. Lamberti, S. Bordiga, G.T. Palomino, C.O. Areán, Catal. Lett. 42 (1996) 25.
[7] G. Socrates, Infrared Characteristic Group Fequencies, second ed., Wiley, New York, 1994, p. 34.
[8] K. Hadjiivanov, J. Saussey, J.L. Freysz, J.C. Lavalley, Catal. Lett. 52 (1998) 103.
[9] H. Feuer (Ed.), The Chemistry of the Nitro and Nitroso Groups, Part 1, Interscience Publishers, New York, 1969, 82 pp.
[10] G. Socrates, Infrared Characteristic Group Fequencies, second ed., Wiley, New York, 1994, p. 42.
[11] A.K. Ghosh, P.A. Kydd, J. Catal. 100 (1986) 185.
[12] Y. Ukisu, S. Sato, G. Muramatsu, K. Yoshida, Catal. Lett. 11 (1991) 177.
[13] Y. Ukisu, S. Sato, A. Abe, K. Yoshida, Appl. Catal. B2 (1993) 147.
[14] V.A. Bell, J.S. Feeley, M. Deeba, R.J. Farrauto, Catal. Lett. 29 (1994) 15.
[15] N.W. Hayes, W. Grünert, G.J. Hutchings, R.W. Joyner, E.S. Shpiro, J. Chem. Soc. Chem. Commun. (1994) 531.
[16] N.W. Hayes, R.W. Joyner, E.S. Shapiro, Appl. Catal. B8 (1996) 343.
[17] C. Yokoyama, M. Misono, J. Catal. 150 (1994) 9.
[18] F. Radtke, R.A. Koeppel, E. Minardi, A. Baiker, J. Catal. 167 (1997) 127.
[19] F. Radtke, R.A. Koeppel, A. Baiker, J. Chem. Soc. Chem. Commun. (1995) 427.
[20] C. Li, K.A. Bethke, H.H. Kung, M.C. Kung, J. Chem. Soc., Chem. Commun. (1995) 813.
[21] F. Poignant, J. Saussey, J.-C. Lavalley, G. Mobilon, J. Chem. Soc. Chem. Commun. (1995) 89.
[22] F. Poignant, J. Saussey, J.-C. Lavalley, G. Mobilon, Catal. Today 29 (1996) 93.
[23] A.W. Aylor, L.J. Lobree, J.A. Reimer, A.T. Bell, Stud. Surf. Sci. Catal. 101 (1996) 661.
[24] T. Beutel, B.J. Adelman, G.-D. Lei, W.M.H. Sachtler, Catal. Lett. 32 (1995) 83.
[25] T. Beutel, B.J. Adelman, W.M.H. Sachtler, Catal. Lett. 37 (1996) 125.
[26] B.J. Adelman, T. Beutel, G.-D. Lei, W.M.H. Sachtler, Appl. Catal. B11 (1996) L1.
[27] Y. Li, T.L. Slager, J.N. Armor, J. Catal. 150 (1994) 388.
[28] T. Tanaka, T. Okuhara, M. Missono, Appl. Catal. B4 (1994) L1.
[29] C. Gaudin, D. Duprez, G. Mabilon, M. Prigent, J. Catal. 160 (1996) 10.
[30] E.A. Lombardo, G.A. Sill, J.L. d'Itri, W.K. Hall, J. Catal. 173 (1998) 440.
[31] A.D. Cowan, N.W. Cant, B.S. Haynes, P.F. Nelson, J. Catal. 176 (1998) 329.
[32] J. March, Advanced Organic Chemistry: Reactions, Mechanisms, and Structure, second ed., McGraw–Hill, New York, 1977.
[33] S. Califano, W. Lüttke, Z. Phys. Chem. Neue Folge 6 (1956) 83.